



ELSEVIER

Available online at www.sciencedirect.com

SCIENCE @ DIRECT®

Earth and Planetary Science Letters 211 (2003) 311–327

EPSL

www.elsevier.com/locate/epsl

Correlation of Indian Ocean tephra to individual Oligocene silicic eruptions from Afro-Arabian flood volcanism¹

Ingrid Ukstins Peate^{a,b,*}, Joel A. Baker^a, Adam J.R. Kent^a,
Mohamed Al-Kadasi^c, Abdulkarim Al-Subbary^c, Dereje Ayalew^d,
Martin Menzies^b

^a Danish Lithosphere Centre, Øster Voldgade 10-L, 1350 Copenhagen K, Denmark

^b Department of Geology, Royal Holloway University of London, Egham, Surrey TW20 0EX, UK

^c Department of Geology, Faculty of Science, Sana'a University, P.O. Box 1247, Sana'a, Yemen

^d Department of Geology, Addis Ababa University, P.O. Box 1176, Addis Ababa, Ethiopia

Received 16 October 2002; received in revised form 20 December 2002; accepted 28 March 2003

Abstract

Widespread silicic pyroclastic eruptions of the Oligocene Afro-Arabian flood volcanic province (ignimbrites and airfall tuffs) produced up to 20% of the total flood volcanic stratigraphy ($>6 \times 10^4$ km³). Volumes of individual ignimbrites and tuffs exposed on land range from ~ 150 to >2000 km³ and eight major units (15–100 m thick) were erupted in <2 Myr, placing these amongst the largest-magnitude silicic pyroclastic eruptions on Earth. They are compositionally distinctive time-stratigraphic markers which were deposited as co-ignimbrite ashfall deposits on a near-global scale around the time of the Oi2 cooling anomaly at ~ 30 Ma. Two ignimbrites from the lower part of the flood volcanic succession in Yemen have been correlated to: (a) the conjugate rifted margin of Ethiopia (>500 km distant); and (b) to two deep sea ash layers sampled by ODP Leg 115 in the Indian Ocean ~ 2700 km to the southeast. This correlation is based on whole rock analyses of silicic units for isotope ratios (Pb, Nd) and rare earth element compositions, in conjunction with novel in situ Pb isotope laser ablation multicollector inductively coupled plasma mass spectroscopy analysis of groundmass and glass shards. Compositional diversity preserved on the scale of individual ash shards in these deep sea tephra layers record chemical heterogeneity present in the silicic magma chambers that is not evident in the welded on-land deposits. Ages of the ash layers can be established by correlation to precisely dated on-land ignimbrites, and current evidence suggests that while these eruptions may have exacerbated already changing climatic conditions, they both marginally post-date the Oi2 global cooling anomaly.

© 2003 Elsevier Science B.V. All rights reserved.

Keywords: Yemen; Ethiopia; Indian Ocean; flood volcanism; silicic volcanism; ignimbrite; tephrochronology; in situ Pb isotope laser ablation

* Corresponding author. Tel.: +45-38-14-26-39; Fax: +45-33-11-08-78.

E-mail address: iau@dlc.ku.dk (I. Ukstins Peate).

¹ Supplementary data associated with this article can be found at [doi:10.1016/S0012-821X\(03\)00192-4](https://doi.org/10.1016/S0012-821X(03)00192-4)

1. Introduction

Continental flood volcanism is characterized by large volumes of basaltic volcanism and, in some cases, silicic volcanism, which are attributed to have high eruption rates over a short time interval ($\sim 1\text{--}3$ Myr [1,2]), and extensive lateral distribution (e.g. 3.9×10^6 km² for Siberian Traps [3–5]). It has been suggested that basaltic and silicic flood volcanism are associated with emissions of SO₂, CO₂, HF and the generation of atmospheric aerosols and particulates which may, in turn, serve as a trigger for climatic disruption and precipitate mass extinction events [6–8]. In Yemen, voluminous silicic ignimbrites (150 to >2000 km³ [9]) were erupted from 30 to 28 Ma [10], and have been linked to silicic ash layers in Indian Ocean drill cores based on paleomagnetic studies [11,12]. In this paper, we investigate the specific correlation of these tephra to individual on-land ignimbrites associated with flood volcanism in Yemen and Ethiopia.

The objective of this study is to geochemically correlate these ash layers to specific Afro-Arabian silicic ignimbrites of precisely known age [9,10]

and provide a first-order control on (1) the absolute age of the ODP tephra, and (2) the proposed relationship between these large-volume eruptions and the Oi2 global cooling anomaly [11–13]. Thus, we have compositionally fingerprinted ODP tephra, and individual silicic pyroclastic deposits found in Yemen and across the conjugate rifted margin of the Red Sea in Ethiopia. Using novel techniques, including in situ trace element and Pb isotopic analysis, which are powerful tools for tephrostratigraphy [14–16], we have established that the Indian Ocean ashes (1) originate from Afro-Arabian silicic eruptions associated with flood volcanism, (2) are correlated with specific ignimbrite units found in Yemen and Ethiopia, and (3) post-date the Oi2 global cooling event. These correlations also provide a chronological framework for precise and absolute dating of the Oi2 event.

The Oi2 cooling anomaly is one of several global climate change events which occurred in the Oligo–Miocene and is associated with extreme fluctuations in Antarctic ice-sheet volume and global temperature [17], and a period of low diversity in land mammals (e.g. Barberá et al. [18]). It is characterized by a maximum in the $\delta^{18}\text{O}$ record (a proxy for glacioeustasy, Fig. 1) that has been identified globally and integrated with lithostratigraphy, biostratigraphy, and magnetostratigraphy in diverse geographic areas (New Jersey, Europe and central Asia [18–24]). The $\delta^{18}\text{O}$ maximum is linked to the calcareous nanofossil zonation division of NP23 to NP24 [23]. Ash layers preserved in the Indian Ocean (ODP Leg 115) straddle the NP23 to NP24 transition [25,26] and thus may potentially be related to the Oi2 event. However, no definitive links have been established yet between the ash layers and Afro-Arabian silicic flood volcanism, or to the impact of silicic or basaltic flood volcanism on climate change.

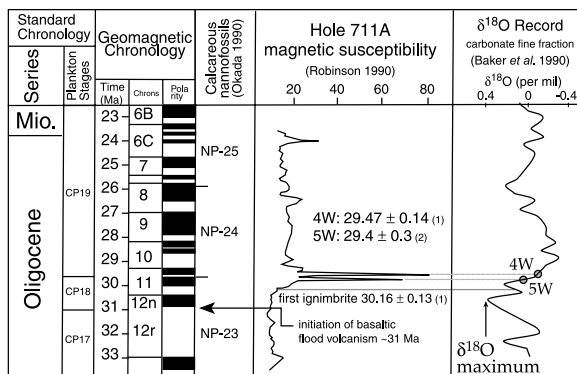


Fig. 1. Calcareous nanofossil zonation, magnetic susceptibility and $\delta^{18}\text{O}$ characterization of ODP Leg 115 cores 711A and 709 ($\delta^{18}\text{O}$) with stratigraphic position of ash layers 5W and 4W annotated [25]. The NP23 to NP24 and CP18 to CP19 transitions occur between 5W and 4W [26]. The generalized geomagnetic chronology is based on Huestis and Acton [57]. Magnetic susceptibility data are after Robinson [27] and ages annotated for 5W and 4W are based on geochemical and isotopic correlations presented in this paper and $^{40}\text{Ar}/^{39}\text{Ar}$ dating of Yemen and Ethiopian flood volcanics (1: Ukstins et al. [9], 2: Baker et al. [10]).

2. Geologic background of tephra and ignimbrites

2.1. Indian Ocean ash layers

ODP Leg 115 Site 711A is located in the west-

ern equatorial Indian Ocean (Fig. 2) and recovered ~250 m of sediment that records deposition from Recent through to the lower-middle Eocene [25]. Two distinct ash layers occur in the upper Oligocene core (Fig. 2): the basal ash (ODP sample notation: ODP core 13X-5W, 10.0–11.0 cm, hereafter referred to as '5W'), is a 5-cm-thick layer disseminated in pelagic sediments located at 120.6 mbsf (meters below sea floor). The overlying ash (13X-4W, 29.0–30.0 cm, hereafter referred to as '4W') is 15 cm thick and occurs at 119.1 mbsf [25]. The transition from plankton zone CP18 to CP19a occurs in the 1.3 m of sediment between these ash layers [26] and, based on average Oligocene sedimentation rates (6–8 m/Ma [25]), 4W is inferred to have been deposited ~160–220 ka after 5W. Site 711 was near or below the carbonate compensation depth (CCD) for most of its depositional history and, thus, foraminifera are absent [25]. However, other sites on this drill leg were located above the CCD during the Oligocene, and ash layers in holes 708, 709 B and C, and 710, which are correlated to 5W and 4W [27], bracket the NP23 to NP24 and the CP18 to CP19a transitions [25] (Fig. 1).

Both ash layers are composed of up to 80% sand-sized grains of volcanic glass (0.25–0.5 mm) with a range of shard morphologies in a nanoplankton ooze matrix. The most common shard types in both ash layers (~60%) are clear tri-cusped bubble junctions, clear planes representing fragmented bubble walls, and clear vesicular glass or whole small bubbles. Pumiceous shards (~10–15%) range from clear to gray in color and many grains have elongate vesicles. A third population of shards is brown (~25–30%) and exhibits a similarly wide range in morphologies, from vesicular and massive transparent glass shards to opaque vesicular shards to moderately vesicular glass particles with botryoidal surface texture. Rare shards have interbanded clear and brown layers. Extremely rare euhedral clinopyroxene crystals are found in 5W, and Touchard et al. [12] also note the presence of very minor amounts of plagioclase and pyroxene crystals.

Ash layers sampled for this study correspond to the upper- and lowermost tephra horizons of the four layers identified by magnetic susceptibility in

ODP Holes 711A and 709B by Touchard et al. [12] (tephra 5W herein = tephra 4, tephra 4W herein = tephra 1). 5W and 4W represent the two largest tephra horizons, and in core 711A where our samples were taken, the two intermediate tephra horizons are present only as minor units, indistinguishable from tephra horizons 5W and 4W based on visual inspection of the core [25]. Both tephra 5W and 4W have normal polarity [12].

2.2. On-shore flood volcanism

The Oligocene Afro-Arabian flood volcanic province is the youngest example of flood volcanic activity associated with continental break-up and inception of ocean spreading, i.e. development of the Red Sea and Gulf of Aden. The bimodal explosive silicic and effusive basaltic volcanism in the province has an estimated volume > 350 000 km³ [28,29] erupted over ~4 Myr (~31–27 Ma [9,10,13,30–33]), with eruption rates comparable to those found on Hawaii today [34]. The province has an areal extent of at least 600 000 km², from southwestern Ethiopia through Eritrea, Djibouti, southern Saudi Arabia and Yemen (Fig. 2).

The Ethiopian Traps contains ~80% of the volume of erupted Oligocene Afro-Arabian flood volcanism [29]. Several recent studies have attempted to characterize the geochemistry [35,36] and the ⁴⁰Ar/³⁹Ar age distribution of silicic flood volcanism [9]. While a generalized stratigraphy does exist [29], no well-defined regional volcanostratigraphy has been established yet because the traps have been extensively faulted and, in places, buried by continuing syn-rift volcanism. In contrast, the volcanostratigraphy of Yemen is well-constrained because flood volcanic sections remain relatively untectonized [37,38] and, apart from volumetrically minor Plio-Quaternary volcanism [39], volcanism effectively ceased on the Yemen rift shoulder after break-up [10]. In Yemen, volcanism was active from 30.9 Ma to 26.7 Ma and the region was uplifted and eroded after continental break-up [10,38]. A composite volcanic stratigraphy, with a total thickness of 1.5 km, has been constructed based on field correlations, petrography and compositional data from

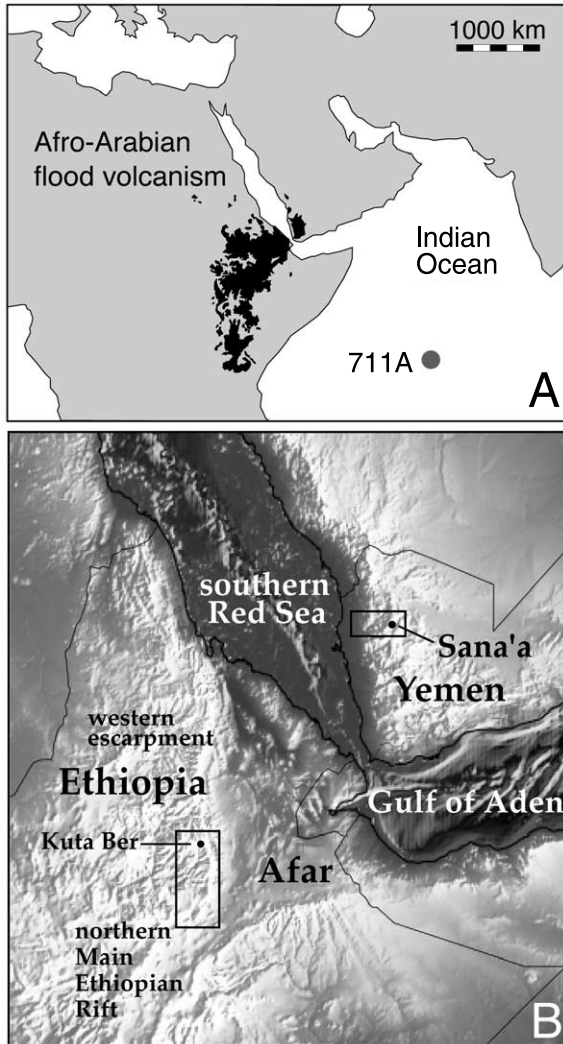


Fig. 2. (A) Map of Afro-Arabia and the Indian Ocean showing the location of the Afro-Arabian flood volcanic province in Yemen and Ethiopia and the site of ODP Leg 115 drill core 711A, where silicic ash layers were recovered that may be associated with Oligocene flood volcanism. (B) Digital elevation model of Afro-Arabia based on a 1-km horizontal grid with ± 30 m vertical resolution. The onshore flood volcanic samples for this study come mainly from the Sana'a area and escarpment of the Yemen plateau (upper box) and from the northern escarpment and northern Main Ethiopian Rift in Ethiopia (lower box). The location of Kuta Ber from the Desi to Bati profile from Ukstins et al. [9] is shown.

eight sections (> 240 sampled ignimbrites, tuffs, silicic and basaltic lavas) from the escarpment to the Sana'a area of western Yemen (summarized in Fig. 3, Ukstins Peate [40]). This volcanic stratig-

raphy is based on major and trace element concentrations and Nd–Pb isotope ratios for a sample set of > 450 silicic ignimbrites and tuffs [40]. Most units are compositionally homogeneous, based on 2–15 major and trace element analyses of samples from multiple sections for each major unit, and are not significantly affected by the presence of lithic material or crystals. At least eight major silicic ignimbrites and tuffs have been identified that can be correlated throughout Yemen, and there are an additional nine silicic units, not present in all sections, that may represent more laterally restricted deposits or have been locally eroded after emplacement. Data from Ethiopia are also used for comparison and they include samples from the Kuta Ber section of the Desi to Bati profile (Ukstins et al. [9], summarized in Figs. 2 and 3) plus a compilation of the regionally sampled suites of Ayalew [35], Ayalew et al. [36], and Ukstins Peate [40]. The Ethiopian data allow us to evaluate spatial variations in volcanic activity across the province and to construct a province-wide volcanostratigraphy that enables correlation of individual silicic units from Yemen to Ethiopia.

3. Analytical methods

3.1. Major element data

The ODP drill core samples were repeatedly rinsed in deionized water, and the ooze matrix decanted off. The remaining bulk ash samples were then dried. Ash shards from each morphological type were hand-picked, and mounted in epoxy for electron microprobe and trace element laser ablation inductively coupled plasma mass spectrometry (ICP-MS) analyses. Major element data on the different shard populations from each ash layer (5W and 4W) were measured by electron microprobe on a representative selection of 3–10 grains of different morphologies (clear shards, clear pumice, dark pumice, and brown shards; Table 1 and Appendix 1¹). Analyses

¹ See online version of this paper.

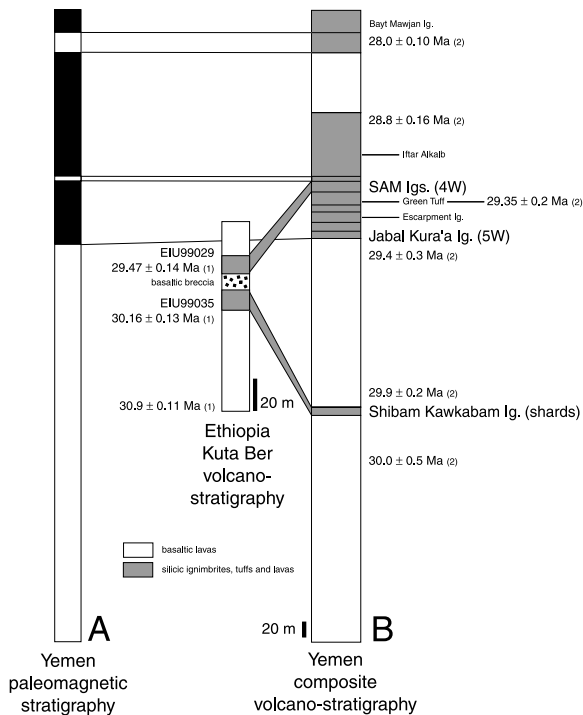


Fig. 3. (A) Paleomagnetic data for Yemen flood volcanism, based on Riisager et al. [55] and DLC unpublished data. Paleomagnetic data are linked to the Yemen composite volcano-stratigraphy, presented in B. (B) Generalized volcanic stratigraphy of Yemen flood volcanism, showing the main basaltic sequence (bottom half of column, white) with the lowermost Shibam Kawkabam Ignimbrite in the middle of the lower basaltic sequence, overlain by the main silicic succession. Ages annotated on the volcanostratigraphy are all $^{40}\text{Ar}/^{39}\text{Ar}$ ages from (1) Uktstins et al. [9] and (2) Baker et al. [10]. Ages from Baker et al. [10] have been recalculated to the Fish Canyon sanidine standard age of 28.02 Ma after Renne et al. [60]. Note the change in vertical scale between the Ethiopian and Yemen stratigraphic sections. The presence of 4W (SAM L) in Ethiopia as well as Yemen suggests it was a bigger eruption, consistent with the thicknesses in the ODP cores (15 cm versus 5 cm for 5W).

were conducted at Århus University, Denmark, using a JEOL JXA-8600 Superprobe with an accelerating voltage of 15 kV and an electron beam of 15 nA defocused to 10 μm to avoid sample devolatilization. Analysis totals ranged from 94 to 98% before normalization to 100%, and given that the glass shards are likely to be hydrated it is difficult to assess the reliability of Na contents. The concentrations of major element oxides

were calculated by reference to a range of oxide and mineral standards. Compositions of ODP tephra glass shards were compared with the compositions of glass or equivalent juvenile material from the on-land ignimbrite and tuff units.

A subset of ~ 5 shards from each of these populations were analyzed by in situ laser ablation methods for trace element abundances and Pb isotopic compositions (Table 2¹ and Appendix 1¹). While electron microprobe and trace element analyses were carried out on the same shards to characterize fully individual shard compositions, the small shard size precluded laser ablation Pb isotope analysis on shards which had been analyzed by laser ablation for trace and rare earth elements (REE), so a different subset of shards was analyzed for Pb isotope ratios by in situ laser ablation multicollector ICP-MS analysis.

3.2. In situ trace element analyses

Laser ablation ICP-MS trace element analyses were performed on ash shards from 5W and 4W using an Elan II quadrupole ICP-MS (at the Geological Survey of Denmark and Greenland, Copenhagen, Denmark) coupled to a Cetac LSX 200 266-nm frequency-quadrupled Nd-YAG laser operated in Q-switched mode. During ablation, an argon carrier gas (flow rate ~ 1 l/min) was used to transfer ablated material to the ICP torch. Each analysis consisted of sequential scanning of the following isotopes: ^{42}Ca , ^{47}Ti , ^{51}V , ^{85}Rb , ^{88}Sr , ^{89}Y , ^{90}Zr , ^{93}Nb , ^{138}Ba , ^{139}La , ^{140}Ce , ^{145}Nd , ^{147}Sm , ^{151}Eu , ^{163}Dy , ^{168}Er , ^{173}Yb . Each analysis consisted of five sweeps through this mass table. Interferences of light REE (LREE) oxides on heavy REE (HREE) peaks were monitored separately and LREE oxide production was found to be negligible ($\text{LREEO}^+/\text{LREE} < 1\%$). In order to maximize signal size and stabilize relative elemental fractionation, analyses were conducted by rastering the laser slowly across each shard at 5–10 $\mu\text{m}/\text{s}$ during ablation. Ablation was conducted using a laser spot size of 50–100 μm , with a laser frequency of 10–15 Hz and energy of 10–15 mJ/cm^2 . Trace element contents were calculated relative to NBS SRM 612 glass using the values of Pearce et al. [15].

Table 1
Average major element data for different shard morphologies (data normalized to 100%)

Ash layer	4W avg	S.D.						
Morphology	ds		dp		cp		cs	
Rock type	trachyte		rhyolite		rhyolite		rhyolite	
No. of shards (<i>n</i>)	5		5		3		9	
SiO ₂	67.72	1.63	70.42	0.93	71.74	0.69	73.23	1.76
TiO ₂	0.88	0.08	0.73	0.12	0.53	0.08	0.53	0.13
Al ₂ O ₃	15.88	1.38	14.75	0.44	14.31	0.40	13.74	0.99
Fe ₂ O ₃	3.83	0.50	3.03	0.41	2.46	0.18	2.42	0.43
MnO	0.24	0.02	0.21	0.05	0.16	0.02	0.18	0.05
MgO	0.76	0.12	0.53	0.15	0.32	0.07	0.28	0.18
CaO	1.27	0.24	0.84	0.25	0.51	0.09	0.47	0.23
Na ₂ O	4.81	0.49	4.47	0.47	3.82	0.32	3.92	0.40
K ₂ O	4.61	0.39	5.04	0.62	6.15	0.51	5.23	0.59
Nb	152	25	158	16	182	15	202	31
Zr/Nb	10.93		10.85		10.29		8.32	
La/Nb	1.2		1.1		1.1		0.9	
Ash Layer	5W avg	S.D.						
Morphology	ds		dp		cp		cs	
Rock type	rhyolite		rhyolite		rhyolite		rhyolite	
No. of shards (<i>n</i>)	3		6		5		10	
SiO ₂	70.93	0.64	71.26	2.56	76.08	1.14	77.02	0.88
TiO ₂	0.97	0.04	0.88	0.28	0.44	0.04	0.38	0.07
Al ₂ O ₃	12.92	0.46	13.04	0.66	11.70	0.32	11.57	0.30
Fe ₂ O ₃	4.23	0.15	4.03	0.89	2.52	0.42	2.27	0.35
MnO	0.14	0.03	0.14	0.07	0.14	0.04	0.11	0.03
MgO	0.80	0.09	0.65	0.36	0.18	0.07	0.13	0.05
CaO	1.49	0.42	1.14	0.65	0.29	0.09	0.21	0.03
Na ₂ O	3.61	0.16	3.75	0.38	3.17	0.26	3.54	0.13
K ₂ O	4.91	0.23	5.11	0.65	5.48	0.53	4.77	0.18
Nb	95	16	115	9	147	14	151	8
Zr/Nb	9.76		10.50		9.99		9.54	
La/Nb	1.2		1.2		1.0		0.9	

ds = dark shard, dp = dark pumice, cp = clear pumice, cs = clear shard; all data in wt%.

Summary of electron microprobe analyses of ODP ash shard populations from 5W and 4W. Average analyses for each shard type are presented here and individual analyses for each shard (*n* = 46) are presented in the supplementary data set. Rock type is based on TAS classification after Le Bas et al. [59]. The standard deviation is ± 2 S.D. All major element analyses reported in the text and tables of this paper are recalculated to 100% anhydrous. Pre-normalized totals ranged from 94 to 98%.

3.3. Pb isotope analyses

Pb isotope analyses were performed with two different methods: (1) MC-ICP-MS analysis using a ²⁰⁷Pb–²⁰⁴Pb double spike (Baker et al. [43]) of solutions of Pb separated from samples by conventional anion exchange chemistry. Bulk clear glass shard samples from 5W and 4W, plus samples of crystal and lithic-free groundmass chips from 20 major Yemen and Ethiopian on-land ignimbrites were analyzed by Pb double spike

methods. (2) Laser ablation MC-ICP-MS analysis – with this method crystal and lithic-free juvenile ignimbrite and tuff groundmass chips or glass shards were ablated with a 266-nm Nd–YAG laser and analyzed with an AXIOM MC-ICP-MS (at the Danish Lithosphere Centre, Copenhagen, Denmark). Samples were prepared by adhering ash shards (~20 per tephra unit) and ignimbrite groundmass chips (~2–5 per sample for >250 samples from Yemen and Ethiopia) onto a clean glass thin section using double-sided adhesive

tape. For each sample, we acquired from 1 to 3 analyses per shard or chip. Average ash analyses are presented in Table 2¹, and average Yemen and Ethiopian ignimbrite data are presented in the supplementary data set. Mass bias was corrected by reference to that observed in analyses of an interspersed glass standard (NIST610). Willigers et al. [41] and Baker et al. [42] have shown that mass bias is essentially matrix independent in a wide variety of materials (glass, phosphates, titanates, silicates, metal) and that this approach, Pb content permitting, can produce data with accuracy and precision that are equivalent to conventional TIMS data. The excellent agreement between our double spike and laser ablation Pb isotope data for the same materials (see Fig. 6D) also verifies the validity of this approach.

3.4. Isotope dilution REE and Nd isotope analyses

Bulk samples (~100 mg) of picked clear glass shards from 5W and 4W and crystal and lithics-free chips from ignimbrite and tuff juvenile ash groundmass were analyzed for Nd isotope ratios and REE concentrations (21 and 19 samples, respectively). Prior to dissolution, bulk ash shard samples were leached for 4 min in a weak acid (0.5 M HNO₃) to clean the shards of adhering siliceous ooze or manganese coatings and to minimize any seawater alteration signature. Ash samples were aliquoted after digestion for REE isotope dilution analysis (after Baker et al. [44]) and Nd isotopes (after Ulfbeck et al. [45]), and an aliquot of the solution was also analyzed for Pb isotope ratios. Clear shards were used for bulk analyses because they are the volumetrically dominant shard type in both ash layers and also because electron microprobe data demonstrated that these populations have relatively homogeneous major element compositions (Table 1).

4. Results

Major element analyses show that although the ash layers (4W and 5W) are heterogeneous in composition (e.g. SiO₂) when viewed as a whole, each different morphological type of shard is rel-

atively homogeneous within each ash layer (Table 1). Generally, all clear shards and pumice are rhyolitic in composition, and dark shards and pumice are less evolved rhyolitic to trachytic compositions (Fig. 4, Table 1). For all shard types, 5W has higher SiO₂ than 4W, and comparing individual populations from both ash layers, clear shards and pumice from 5W have the highest SiO₂ contents (76–77 wt%), and dark massive glass shards and pumice from 4W have the lowest SiO₂ (67–70 wt%, Fig. 4). On a TAS diagram (Fig. 4) the four shard types found in each ash layer lie along a classic rhyolite fractionation trend with increasing SiO₂ content (although variations are close to analytical error), indicating the transition from anorthoclase to sanidine fractionation occurred at ~72.5 and 74 wt% SiO₂ for 4W and 5W, respectively. At a given SiO₂, 5W is more enriched in TiO₂, Fe₂O₃, MgO and CaO than 4W. TiO₂, Fe₂O₃, MgO and CaO also show consistent trends, decreasing with increasing SiO₂ in each tephra (e.g. Fe₂O₃, Fig. 5).

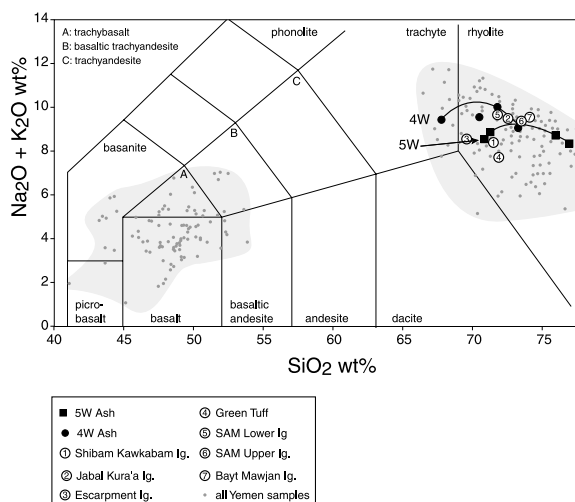


Fig. 4. Total alkalis versus silica diagram after Le Bas et al. [59]. Basaltic lava geochemical data (symbols and background field) are from Baker [37] and Baker et al. [54], basaltic lava and rhyolitic ignimbrite and tuff data are from this study and Ukstins Peate (unpublished data). Four ash shard morphologies (in order of increasing SiO₂: dark shard, dark pumice, clear pumice, clear shard) for each ash layer (5W and 4W) are plotted. Average compositions for the main ignimbrites and tuffs from Yemen are plotted. All data presented here have been screened for LOI < 5 wt%.

Major and trace element concentrations for individual ash shards from each tephra layer preserve coherent and well-defined trends, as shown in Fig. 5. Analyzed shards span a wide range in SiO_2 compositions (68–78 wt%) and represent the full range in morphologic shard types preserved in the ash layers. SiO_2 versus Fe_2O_3 concentrations clearly show that tephtras 5W and 4W are compositionally distinct, and have a curvilinear trend consistent with crystal fractionation as a primary process controlling compositional variations within individual tephtra units (Fig. 5A). SiO_2 versus K_2O and Zr concentrations clearly demonstrate that binary mixing cannot produce the compositional variations observed within the tephtra layers (Fig. 5B,H). Major element data for the four Indian Ocean tephtra layers from Touchard et al. [12] are shown for comparison, where tephtra 4 = our 5W and tephtra 1 = our 4W. It is interesting to note that the two intermediate tephtra layers of Touchard et al. [12] (tephtras 2 and 3), which were not sampled for this study, have major element compositions very similar to our tephtra 4W. While ash shard analyses presented here display tight and coherent trends, data from Touchard et al. [12] do not show such trends. Their average analyses for tephtra 1 (=4W) overlap our data field for ash 4W, and surprisingly their average analyses for tephtra 4 (=5W) also lie within our data field for ash 4W (Fig. 5A).

Pb isotope ratios of shards within each ash layer are homogenous over a wide range in SiO_2 concentrations (Fig. 5C). SiO_2 versus Nb displays a tight positive correlation (Fig. 5D) and indicates Nb was acting as a highly incompatible element. Therefore, Nb can be used as a fractionation index to assess the behavior of other incompatible trace elements such as U, Eu, Ba and Zr: (i) Nb versus U (Fig. 5E) – both tephtra layers show a very tight linear trend of increasing U with increasing Nb. U is usually fluid-mobile, but here is clearly not affected by secondary alteration. Similar observations for other fluid-mobile elements such as K_2O and Ba indicate that these elements are also unaffected by alteration despite the marine depositional environment of the tephtras. (ii) Nb versus Ba, Eu/Eu* (Fig. 5F,G, and Sr, not shown) – both tephtra layers show a significant

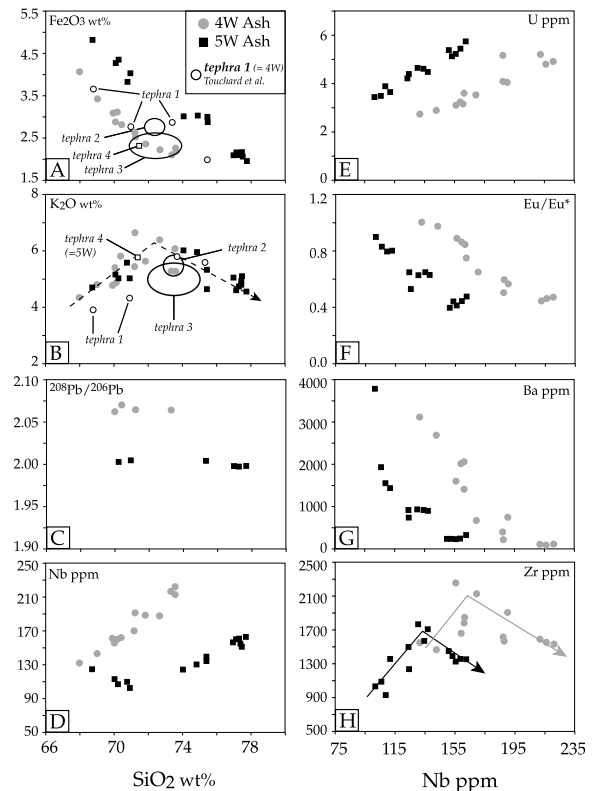


Fig. 5. Major and trace element variations within individual ash shards from the Indian Ocean tephtra layers 5W (black squares) and 4W (gray circles). Curvilinear trends in major and trace elements are consistent with crystal fractionation of feldspar and Fe–Ti oxides. Major element data from Touchard et al. [12] are shown for comparison. Tephtra 5W (lowermost unit) here is equivalent to Touchard et al.’s tephtra 4 (open square), tephtra 4W (uppermost unit) here is equivalent to Touchard et al.’s tephtra 1 (open circles). Touchard et al.’s tephtras 2 and 3 (intermediate two units, shown as large ovals, representing average analyses with standard deviation) were not discussed here, but are geochemically similar to our tephtra 4W based on major element compositions. Data points for tephtras 5W and 4W represent individual shard analyses and show the full range of compositional variations found within each ash layer.

decrease in these elements with increasing Nb, indicating feldspar was a fractionating phase in both magma systems. (iii) Nb versus Zr (Fig. 5H) – each tephtra shows a distinct and sharp increase followed by a decrease in Zr with increasing Nb, corresponding to the onset of zircon fractionation. The start of zircon fractionation occurs

at ca. 135 ppm Nb for ash 5W and 160 ppm Nb for ash 4W, corresponding to SiO₂ concentrations of 75 and 72 wt%, respectively.

Nb concentrations can also be used to approximate the extent of crystallization recorded by the ash shards. Assuming Nb is perfectly incompatible, the observed change in Nb concentrations for ash layers 5W and 4W yield F values of 0.63 and 0.59 respectively, indicating that a *minimum* of 40% fractional crystallization has occurred in order to produce the range of compositions in each tephra layer.

On a Zr/Nb versus La/Nb plot (Fig. 6A), clear glass shards from 5W and 4W fall into two distinct groups with different Zr/Nb ratios (5W: 6.1–6.4, 4W: 4.6–5.0). Some clear pumice grains from each unit also plot with the clear glass shards. For 5W, all other tephra morphologies form a second field at higher Zr/Nb and La/Nb, whereas for 4W the other morphologies form a linear trend extending from the clear shards to higher Zr/Nb and La/Nb (Fig. 6A).

Pb isotope ratios determined by both in situ laser ablation MC-ICP-MS and Pb DS solution work are very distinctive for each tephra layer, and there is excellent agreement between the laser ablation and solution data (Fig. 6C,D). Shards from 5W have low ²⁰⁷Pb/²⁰⁶Pb and ²⁰⁸Pb/²⁰⁶Pb (~0.81 and ~2.00, respectively) and high ²⁰⁶Pb/²⁰⁴Pb values (19.25), whereas 4W shard compositions lie at high ²⁰⁷Pb/²⁰⁶Pb and ²⁰⁸Pb/²⁰⁶Pb (~0.835 and ~2.065, respectively) and lower ²⁰⁶Pb/²⁰⁴Pb (18.77) (Fig. 6E). Two shards, one from each ash layer, are interpreted as a reworked component from an older eruption and form a third, separate group at ²⁰⁷Pb/²⁰⁶Pb and ²⁰⁸Pb/²⁰⁶Pb of ~0.815 and ~2.01 (Fig. 6C). Shards from 5W have negative Δ8/4 [46].

Although Nd isotope ratios are very similar for the two tephra layers (¹⁴³Nd/¹⁴⁴Nd ~0.51285), REE concentrations are different (Fig. 7, Table 2¹). 4W has consistently higher REE concentrations than 5W (Table 2¹). While the general shapes of the REE patterns are similar (Fig. 7D), 4W is more enriched than 5W in light to middle REEs for a given heavy REE content.

A detailed discussion of geochemical compositional variations found in the Oligocene Yemen

ignimbrites and tuffs will be presented in a forthcoming paper on the volcanic stratigraphy.

5. Discussion

5.1. Identifying the source of the Indian Ocean ashes

In addition to Afro-Arabian flood volcanism, other potential sources of silicic pyroclastic eruptions at ~30 Ma were: (1) large-volume silicic ignimbrites from southern North America; (2) arc magmatism; (3) the East African Rift; and (4) the Réunion hotspot track and Kerguelen plume. The East African Rift is thought to have been active in pulses, during the late Eocene (44–38 Ma) and middle Miocene (16–11 Ma [47]) and therefore has been ruled out as a potential source for the Indian Ocean tephra based on age differences. Volcanic products of the Réunion hot spot track, located near ODP Leg 115, have been dominated by effusive basaltic volcanism [48–50] and can also be ruled out as a potential source for the tephra based on the dearth of rhyolitic eruption products found there. Geochemical data from Mexican and arc silicic volcanism [51–53] compared with the ashes 5W and 4W and with the Afro-Arabian flood volcanic province on a ²⁰⁷Pb/²⁰⁶Pb versus La/Nb isotopic plot (Fig. 6B), clearly distinguish the Yemen volcanism and ODP tephra from all global arc lavas (a compilation of Andean, Banda, Cascades, Honshu, Luzon, New Hebrides, Sunda and Vanuatu arc data is used here) and Mexican silicic ignimbrites which plot at significantly higher La/Nb ratios than the Yemen volcanic rocks and ash layers.

In a plot of ²⁰⁷Pb/²⁰⁶Pb versus ²⁰⁸Pb/²⁰⁶Pb (Fig. 6D), Yemen silicic flood volcanic rocks clearly fall into two distinct groups, one with higher ²⁰⁷Pb/²⁰⁶Pb and ²⁰⁸Pb/²⁰⁶Pb ratios ('high Pb': >0.825 and >2.03) and a second group with low ²⁰⁷Pb/²⁰⁶Pb and ²⁰⁸Pb/²⁰⁶Pb ratios ('low Pb': <0.825 and <2.03). The 'low-Pb' group is very distinct and also has a negative Δ8/4 value in ²⁰⁶Pb/²⁰⁴Pb–²⁰⁸Pb/²⁰⁴Pb space [54]. Ash 5W falls into the 'low-Pb' group while most shards from ash 4W fall in the 'high-Pb' group.

In summary, broad similarities in major, trace element and REE concentrations, and Pb isotope ratios, demonstrate that Indian Ocean tephra layers 5W and 4W are likely associated with Afro-Arabian flood volcanism and represent distal airfall tuffs produced during Oligocene explosive silicic eruptions in Yemen and Ethiopia. The question is whether the ash layers can now be linked to specific eruptions from the on-shore record of flood volcanism and thereby provide a more precise age and stratigraphic context for their emplacement.

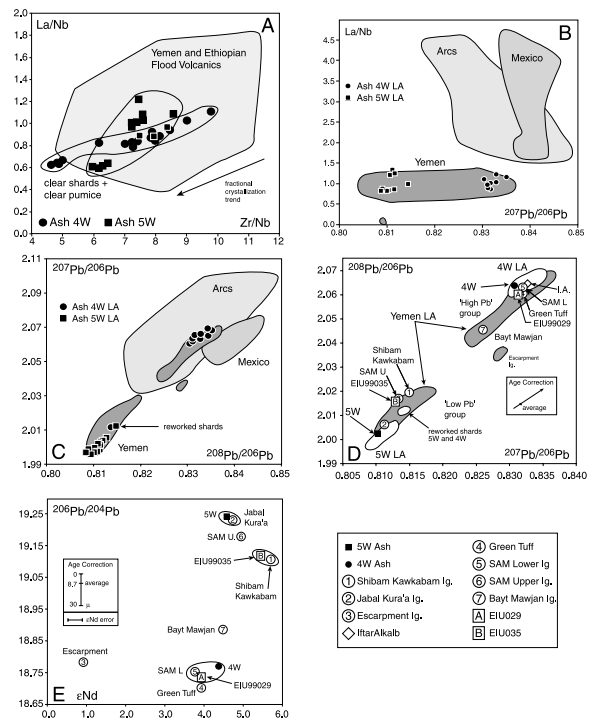
5.2. Correlating individual eruption units

Fig. 3 presents a generalized stratigraphy for Yemen silicic volcanism discussed here and illustrates potential correlations among ash layers 5W and 4W and Afro-Arabian ignimbrites. Several of the main silicic pyroclastic units found in Yemen and Ethiopia lie within the data fields for the ashes defined by laser ablation analyses on a $^{207}\text{Pb}/^{206}\text{Pb}$ versus $^{208}\text{Pb}/^{206}\text{Pb}$ plot (Fig. 6D). 5W can be correlated to the Jabal Kura'a Ignimbrite, the oldest regionally distributed ignimbrite found on the Yemen plateau (Fig. 3).

4W can be correlated to a stratigraphically and chronologically closely related suite of pyroclastic units: (1) a tuff (the Green Tuff), (2) an overlying ignimbrite (SAM Ignimbrite Lower), and (3) a capping mega-breccia (Iftar Alkalb), plus (4) an Ethiopian ignimbrite (sample number EIU99029) (stratigraphic names from Uktstins Peate [40]; see Fig. 3). The Green Tuff is a Plinian tephra fall deposit that is genetically related to the overlying SAM Ignimbrite based on geochemical similarities [40]. The SAM Ignimbrite is especially notable for its distinctive vertical geochemical and isotopic zonations: all of SAM Lower (SAM L) and the lowermost 2/3 of SAM Upper (SAM U) fall in the isotopic 'high-Pb' group while the uppermost 1/3 of SAM U is in the 'low-Pb' group (Fig. 6D). The unit as a whole exhibits continuous zoning in incompatible trace elements such as Zr ($\sim 750\text{--}1100$ ppm) and Nb ($\sim 100\text{--}140$ ppm). This extreme zonation is a diagnostic feature and has also been identified in the Ethiopian ignimbrite EIU99029. Representative compositions for SAM L and

SAM U are used in this study. Iftar Alkalb is a caldera-collapse breccia that is genetically related to the Green Tuff and SAM Ignimbrite based on similarities in major and trace element compositions and Pb–Nd isotope ratios. However, it is only found in the Sana'a area ($22\,500\text{ km}^2$) and, as a localized deposit, it is not considered as a potential source for the Indian Ocean ashes.

The reworked shards found in 5W and 4W can potentially be correlated to: (1) the Yemen Shibam Kawkabam Ignimbrite, the oldest ignimbrite currently identified Yemen, (2) the Ethiopian ignimbrite EIU99035, the oldest ignimbrite currently identified in Ethiopia, and (3) the isotopically distinct top of SAM U (Fig. 3). For 5W, the accidental shards are unlikely to be related to SAM U on stratigraphic grounds, but it cannot be ruled out for 4W because of the genetic link between SAM L and SAM U. The reworked shard population found in ash layers 5W and 4W represent a volumetrically minor component ($< 3\%$). These shards represent either incorporation of older material during a younger eruption



or reworking of ash during sedimentation or bioturbation after deposition on the ocean bottom.

By plotting our tentatively correlated ignimbrites and Indian Ocean ash layers on an ϵ_{Nd} versus $^{206}\text{Pb}/^{204}\text{Pb}$ diagram (Fig. 6E), we can refine the Pb isotopic correlations presented above. Ash layer 5W and the Jabal Kura'a Ignimbrite have high $^{206}\text{Pb}/^{204}\text{Pb}$ ratios and ϵ_{Nd} values (5W: 19.25, +4.6; Jabal Kura'a: 19.23, +4.7; Fig. 6E). Ash 4W, SAM L, the Green Tuff and EIU99029 have similar ϵ_{Nd} values (3.8–4.4) but are easily distinguished from 5W by their markedly different $^{206}\text{Pb}/^{204}\text{Pb}$ composition of ~ 18.73 . Shibam Kawkabam and EIU99035 have distinct, and common, high ϵ_{Nd} values of ~ 5.7 and $^{206}\text{Pb}/^{204}\text{Pb}$ values of ~ 19.1 compared to SAM U, which has a lower ϵ_{Nd} value of 4.9 and higher $^{206}\text{Pb}/^{204}\text{Pb}$ (19.18) (Fig. 6D,E). These isotopic correlations of eruption units (Fig. 6E) now represent stratigraphically and chronologically consistent and coherent packages that can be traced across the conjugate rifted margins of the Red

Sea and also to the Indian Ocean ash layers (Fig. 3).

In a further test of our proposed correlations, Fig. 7 presents REE patterns for each of the three groups of units that are inferred to represent products of the same eruption. Ash 5W and Jabal Kura'a Ignimbrite have near-identical REE patterns (Fig. 7A), albeit displaced to slightly different abundances due to differing proportions of crystals or amounts of fractional crystallization. Similarly, ash 4W has a near-identical REE pattern to SAM L and EIU99029, although the Eu anomalies vary slightly, principally due to the variable bulk content of feldspar phenocrysts found in the whole rock samples as opposed to the phenocryst-free glass shards that have larger negative anomalies. This is supported by the fact that the sample with the largest volume of feldspar phenocrysts ($\sim 12\%$: EIU99029) has the smallest Eu anomaly (Fig. 7B). This variation could be due to ash winnowing from the ignimbrite at a more distal locality. Shibam Kawkabam Ignim-

←

Fig. 6. Geochemical and isotopic diagrams of ash shards and bulk chemical analyses for ODP tephtras 5W and 4W, plus the main Yemen and Ethiopian silicic eruption units. (A) Zr/Nb versus La/Nb. In situ ICP-MS data for single shards from ashes 5W and 4W compared to XRF data on silicic units from Yemen and Ethiopian flood volcanics. Clear shards and clear pumice form a coherent and distinct group for each ash layer which lies along the edge of the main Yemen and Ethiopian data field. Symbols are laser ablation data for the two tephtra layers 5W and 4W; the field is XRF data from a suite of Yemen and Ethiopian silicic flood volcanic rocks ($n = > 240$). (B) $^{207}\text{Pb}/^{206}\text{Pb}$ versus La/Nb. In situ shard laser ablation Pb isotopes and REE for single shards compared with laser ablation and XRF data from Yemen silicic volcanics and a global database of arc volcanism and silicic volcanism from southern North America [52,53]. For arc magmatism we use a compilation incorporating > 2000 analyses from the Andean, Banda, Honshu, Vanuatu, Sunda, Cascades and Luzon arcs (<http://georoc.mpch-mainz.gwdg.de>) that was screened for volcanic rocks with $\text{SiO}_2 > 60\%$. The Indian Ocean ash shards are clearly distinguished from Mexican and arc sources of silicic volcanism and overlie the field of Afro-Arabian flood volcanism. Symbols are laser ablation data; Yemen field is XRF and laser ablation data; other fields are published data sets. (C) $^{207}\text{Pb}/^{206}\text{Pb}$ versus $^{208}\text{Pb}/^{206}\text{Pb}$. Pb laser ablation data from ash layers 5W and 4W plotted with Yemen laser ablation data. Yemen data define two groups, one 'low-Pb' group and one 'high-Pb' group (see text for discussion). One ash layer falls into each of these fields. Several ash shards from both 5W and 4W form an isotopically distinct group in the 'low-Pb' field, and may be shards from an older eruption which were incorporated into subsequent younger eruptions. Symbols are laser ablation data; Yemen field is laser ablation data; other fields are published data sets. (D) $^{207}\text{Pb}/^{206}\text{Pb}$ versus $^{208}\text{Pb}/^{206}\text{Pb}$: Pb DS data for major Yemen and Ethiopian silicic pyroclastic units compared with Pb DS data for the ash layers and Pb laser ablation data fields for the ash layers and for all Yemen silicic pyroclastic rocks. Errors on Pb DS data are smaller than the symbols. Age correction vectors are shown and average corrections are marked on the vectors. Data are not age corrected. Comparison of laser ablation and Pb double spike data for 5W and 4W; double spike data for bulk shard analyses lie within the laser ablation fields for each ash layer, showing that a good agreement exists between the laser data and high-precision Pb double spike data. Ash 5W is correlated to Jabal Kura'a Ignimbrite, ash 4W is correlated to SAM L, Green Tuff and EIU99029, and accidental ash shards from 5W and 4W are correlated to Shibam Kawkabam Ignimbrite (5W), EIU99035 (5W) and SAM U (4W). (E) ϵ_{Nd} versus $^{206}\text{Pb}/^{204}\text{Pb}$. This plot supports correlations based on $^{207}\text{Pb}/^{206}\text{Pb}$ versus $^{208}\text{Pb}/^{206}\text{Pb}$. Ash 5W+Jabal Kura'a Ignimbrite, ash 4W+SAM L+EIU99029, and Shibam Kawkabam+EIU99035 can be correlated and represent individual eruptions distributed across Afro-Arabia and deposited in the Indian Ocean. Pb isotope data are not age corrected and the average age correction is shown, which is typically smaller than the symbol size. Nd isotope data are age corrected and errors are shown.

brite and EIU99035 have identical REE patterns, EIU99035 having slightly higher REE contents, and both are distinctly different from the ODP ash layers (5W is shown for comparison, Fig. 7C).

Because the differences in REE patterns between units are relatively small, we have carried out residuals calculations comparing the REE concentrations of the two ash layers with 16 ignimbrites from Yemen and Ethiopia, and these strongly support the proposed correlations (see supplementary data set for results and calculation details). The Jabal Kura'a Ignimbrite has the lowest residual difference from 5W (sum of squared residuals of La–Lu concentration: 0.008), com-

pared to any other Yemen or Ethiopian ignimbrite. Residuals comparing ignimbrites to 4W show more complexity. The two units correlated on the basis of major and trace element compositions and isotope ratios have sums of the squared residuals of 0.165 (SAM L) and 0.202 (EIU99029). Excluding the Eu residual, which is controlled by feldspar fractionation in the Yemen–Ethiopian ignimbrites, these two units have the lowest residuals for 4W. Thus the residual data indicate that the ash layer 4W is correlated to the lower part of the SAM Ignimbrite (i.e. SAM L). Thus, the only differences in REE between the ash layers and the units correlated to

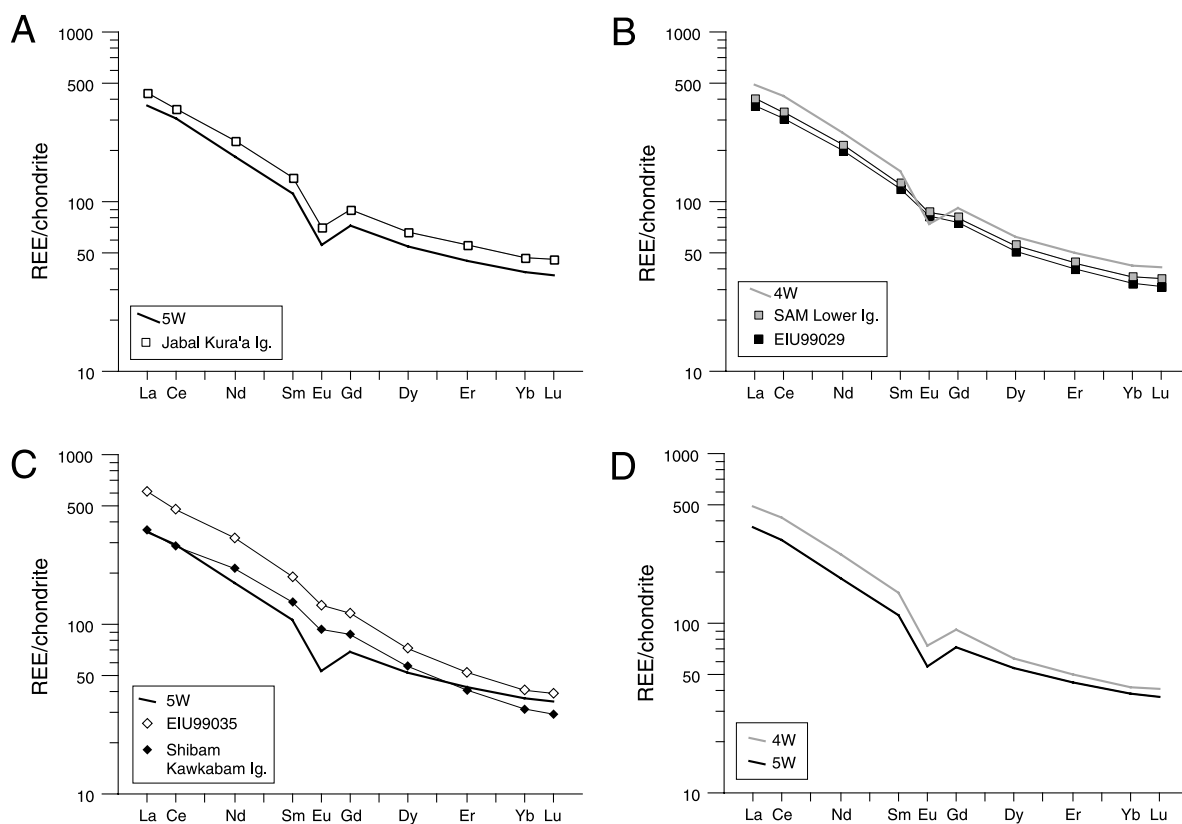


Fig. 7. (A) REE concentrations for ODP ash 5W and Yemen Jabal Kura'a Ignimbrite normalized to chondrite values of Anders and Grevesse [61]. (B) REE concentrations for ODP ash 4W, Yemen SAM L Ignimbrite and Ethiopian ignimbrite EIU99029 normalized to chondrite values of Anders and Grevesse [61]. (C) REE concentrations for Yemen Shibam Kawkabam Ignimbrite and Ethiopian ignimbrite EIU99035 normalized to chondrite values of Anders and Grevesse [61]. A bulk REE pattern from ash 5W is shown for comparison. (D) REE concentrations for ODP ash layers 5W and 4W normalized to chondrite values of Anders and Grevesse [61] are shown for comparison. Note the higher LREE to middle REE concentrations in 4W compared to 5W for a given HREE. Residual differences between 5W and 4W REE concentrations are presented in the supplementary data set.

them are the absolute REE contents and the relative Eu concentrations, which is a function of feldspar fractionation or accumulation. Therefore, the REE data are remarkably consistent with the geochemical correlations based on major and other trace element compositions and isotope ratios.

The correlation of the tephra layers 5W and 4W to the on-land Jabal Kura'a and SAM Ignimbrites is entirely consistent with stratigraphic relationships, paleomagnetic data from the ODP drill cores [12], and $^{40}\text{Ar}/^{39}\text{Ar}$ dating and paleomagnetic studies from Yemen and Ethiopian on-land ignimbrites [9,10,55] (Fig. 3). Of the two intermediate ash layers identified by Touchard et al. [12], both have major element concentrations that resemble our tephra 4W and most likely correlate to the Yemen Green Tuff that immediately underlies the SAM Ignimbrite (Fig. 3). Touchard et al. [12] attempt to link the Indian Ocean tephra to silicic ignimbrites found in the Lima Limo section of Ethiopia. However, this correlation is invalid based on very distinctive Pb isotopic ratios for the Lima Limo ignimbrites ($^{207}\text{Pb}/^{206}\text{Pb}$: 0.8667, $^{208}\text{Pb}/^{206}\text{Pb}$: 2.085 [40]).

5.3. Magma compositional heterogeneity preserved in shards

Ash layers 5W and 4W exhibit compositional heterogeneity on several scales. Different morphologic shard populations have variable major and trace element compositions (Tables 1 and 2¹); some element concentrations vary by > 500%. For example, in ash layer 5W, Ba in clear shards is 367 ppm (± 301), versus 2067 ppm (± 1040) in brown glass. Even relatively immobile elements such as Zr range from 470–1355 ppm in dark shards and 821–1706 ppm in clear shards (both from 5W, representing an average Zr enrichment of $\sim 150\%$ in the clear shards). Individual shards within different subgroups can be highly distinctive in terms of trace element compositions. As presented above, in ash 5W, Ba in clear shards varies from 230 to 3790 ppm, but of the six shards analyzed four had values of 234 ± 4 ppm, one had a value of 905 ppm and one had a value of 3790 ppm. Relatively few highly enriched shards cause a significant amount of scatter. In addition, rare

reworked shards with distinct Pb isotope ratios are found in both 5W and 4W. While variability in elements such as Ba and Sr (Table 2¹, supplementary data set) may be a result of secondary alteration or interaction with seawater, variations in immobile elements such as Zr are likely to reflect primary compositions. Coherent trends between major and trace elements are consistent with tapping a strongly zoned rhyolitic magma chamber. Evidence for the existence of zoned magma chambers can be found in the chemical zonation of the SAM Ignimbrite, as well as in the shards themselves (Fig. 5). Because the tephra units are preserved as diffuse horizons from 10 to 15 cm thick within siliceous ooze sediments, rather than as discrete and concentrated ash layers, it is plausible that these layers preserve shards from multiple eruptions, as has been suggested by Touchard et al. [12]. Based on deposition rates, a 10-cm layer of siliceous ooze is likely to represent ~ 14 ka [25]. However, we interpret these mixed populations of shards from the individual ash layers 5W and 4W to represent tephra derived from two main eruption events of very short duration (days to weeks), which is supported by the relatively homogeneous Pb laser ablation isotope compositions of shards within individual layers (Fig. 5).

5.4. Volume estimates

Volumes of individual silicic pyroclastic units erupted during flood volcanism vary over an order of magnitude for the Yemen plateau. The Jabal Kura'a Ignimbrite has an estimated volume of ~ 200 km³. The Green Tuff and SAM Ignimbrite have an estimated combined minimum volume of ~ 1200 km³ in Yemen, and when the correlation to Ethiopia is taken into account, the estimated volume increases to ~ 1500 km³. Touchard et al. [56] identified ash layers from the Arabian Sea, South Atlantic Ocean, the Tasman Sea and Gubbio, Italy, that occur at an identical interval to the ashes found in Leg 115, and they propose that these layers are correlated to Afro-Arabian silicic eruptions based on temporal similarities and paleomagnetic data. Geochemical correlations and Pb isotopic fingerprinting, which should be possi-

ble with the stratigraphic and geochemical framework presented here, can be used to confirm that these ash layers represent more distal deposits of the same units we have discussed, and that Afro-Arabian silicic pyroclastic eruptions were emplaced on a near-global scale. If this is the case, then eruption volumes may be significantly larger ($>200\%$) than previously estimated, and potentially $>3000\text{ km}^3$.

5.5. Age of the Indian Ocean ash layers and relationship to the Oi2 cooling event

An internally consistent $^{40}\text{Ar}/^{39}\text{Ar}$ chronostratigraphy for Yemen silicic and basaltic units intercalated with the Jabal Kura'a and SAM Ignimbrites suggests SAM is ~ 100 kyr younger than Jabal Kura'a Ignimbrite (Fig. 3, [10]). This is in excellent agreement with the ~ 190 kyr age difference between tephros 5W and 4W calculated using average sedimentation rates in the ODP cores [25]. Reworked shards found in 5W and 4W, correlated to the first regional ignimbrite in the Afro-Arabian flood volcanic province (Shibam Kawkabam Ignimbrite and EIU99035), were erupted at 30.16 ± 0.13 Ma (based on a date for EIU99035 [9]). Ash 5W, which has been correlated to the Jabal Kura'a Ignimbrite, is 29.4 ± 0.3 Ma [10], and ash 4W, correlated to the SAM Ignimbrite and EIU99029, was erupted at 29.47 ± 0.14 Ma [9,10].

Based on inherent errors in the chronostratigraphic timescale (± 0.5 Ma [57]) and the results of a radiometric age calibration of the Eocene–Oligocene biostratigraphy [19], Uktins et al. [9] suggested silicic flood volcanism post-dated the Oi2 global cooling event by 0.2–1.6 Myr. The proposed asynchrony depends in part on the accuracy of the time scale calibration. By establishing a geochemical correlation between the Indian Ocean ash layers and Afro-Arabian flood volcanism we provide a means to link the chrono-, magneto- and biostratigraphic records. Baker et al. [58] examined isotopic ratios in the carbonate fine fraction from Site 709, and found a peak in $\delta^{18}\text{O}$ distinctly below 5W that seems to indicate that the Oi2 cooling anomaly pre-dates the emplacement of the ash layers (Fig. 1). Baker et al.

[58] also state that diagenetic changes and climate changes produce similar results to those observed in the $\delta^{18}\text{O}$ and Sr isotope records from this site, and it is not straightforward to differentiate between the two. However, based on the evidence at hand, we suggest silicic flood volcanism post-dates any major climatic cooling event, and suggest that it is impossible to unequivocally establish a causal link even if there were a temporal relationship. Nevertheless, it is plausible that such voluminous silicic pyroclastic eruptions may have accelerated climatic variations.

6. Summary

1. Major and trace element and REE abundances and Pb–Nd isotopic ratios indicate that ash layers found in ODP Leg 115 cores in the Indian Ocean originated from two of the oldest, large-volume silicic pyroclastic eruptions of the Oligocene Afro-Arabian flood volcanic province.
2. We can unequivocally demonstrate that these ashes are geochemically correlated to specific silicic volcanic eruptions from Yemen and can also correlate these individual eruption units across the Red Sea to the conjugate rifted margin of Ethiopia.
3. Correlation to $^{40}\text{Ar}/^{39}\text{Ar}$ -dated ignimbrites in Yemen [10] and Ethiopia [9] provides age constraints for the ashes: (1) 5W (oldest): 29.4 ± 0.3 Ma, and (2) 4W (youngest): 29.47 ± 0.14 Ma. These ages can be used to link on-land and marine bio- and magnetostratigraphy and tephrochronology studies.
4. Afro-Arabian silicic flood volcanism post-dates the Oi2 global cooling event.

Acknowledgements

I.U.P. was supported by a joint Ph.D. fellowship from the Danish Lithosphere Centre and Royal Holloway University of London. The Danish Lithosphere Centre is funded by the Danish National Research Council. We thank Tod Waight for support in the MC-ICP-MS Labora-

tory at the Danish Lithosphere Centre, and Christian Tegner and Sidsel Grundvig for assistance with electron microprobe analyses at Århus University. Jørgen Kystol assisted with ICP-MS analysis at the Geocenter, Copenhagen. We thank Hans Christian Larsen for informative discussions and David W. Peate for useful critiques. Steve Sparks and Steven Self are thanked for their constructive reviews that improved this paper. [BW]

References

- [1] M.A. Richards, R.A. Duncan, V.E. Courtillot, Flood basalts and hot-spot tracks plume heads and tails, *Science* 246 (1989) 103–107.
- [2] I.H. Campbell, R.W. Griffiths, Implications of mantle plume structure for the evolution of flood basalts, *Earth Planet. Sci. Lett.* 99 (1990) 79–93.
- [3] M.K. Reichow, A.D. Saunders, R.V. White, M.S. Pringle, A.I. Al'Mukhamedov, A.I. Medvedev, N.P. Kirda, $^{40}\text{Ar}/^{39}\text{Ar}$ dates from the West Siberian Basin Siberian flood basalt province doubled, *Science* 296 (2002) 1846–1849.
- [4] R.S. White, D.P. McKenzie, Magmatism at rift zones: The generation of volcanic continental margins and flood basalts, *J. Geophys. Res.* 94 (1989) 7685–7729.
- [5] M.F. Coffin, O. Eldholm, Large igneous provinces: Crustal structure, dimensions, and external consequences, *Rev. Geophys.* 32 (1994) 1–36.
- [6] O. Eldholm, E. Thomas, Environmental impact of volcanic margin formation, *Earth Planet. Sci. Lett.* 117 (1993) 319–329.
- [7] S. Self, T. Thorvaldur, L. Keszthelyi, Emplacement of continental flood basalt lava flows, in: Mahoney, J.J., Coffin, M.F. (Eds.), *Large Igneous Provinces*, Geophysical Monograph 100, Am. Geophys. Union, Washington, DC, 1997, pp. 381–410.
- [8] P.B. Wignall, Large igneous provinces and mass extinctions, *Earth Sci. Rev.* 53 (2001) 1–33.
- [9] I.A. Ukstins, P.R. Renne, E.W. Wolfenden, J. Baker, D. Ayalew, M. Menzies, Matching conjugate volcanic rifted margins: $^{40}\text{Ar}/^{39}\text{Ar}$ chrono-stratigraphy of pre- and syn-rift bimodal flood volcanism in Ethiopia and Yemen, *Earth Planet. Sci. Lett.* 198 (2002) 289–306.
- [10] J. Baker, L. Snee, M. Menzies, A brief Oligocene period of flood volcanism in Yemen: implications for the duration and rate of continental flood volcanism at the Afro-Arabian triple junction, *Earth Planet. Sci. Lett.* 138 (1996) 39–55.
- [11] P. Rochette, E. Tamrat, G. Feraud, R. Pik, V. Courtillot, E. Ketefo, C. Coulon, C. Hofmann, D. Vandamme, G. Yirgu, Ethiopian traps, *Earth Planet. Sci. Lett.* 164 (1998) 497–510.
- [12] Y. Touchard, P. Rochette, M.P. Aubry, A. Michard, High-resolution magnetostratigraphic and biostratigraphic study of Ethiopian traps-related products in Oligocene sediments from the Indian Ocean, *Earth Planet. Sci. Lett.* 206 (2003) 493–508.
- [13] C. Hofmann, V. Courtillot, G. Feraud, P. Rochette, G. Yirgu, E. Ketefo, R. Pik, Timing of the Ethiopian flood basalt event and implications for plume birth and global change, *Nature* 389 (1997) 838–841.
- [14] C.J. Bryant, R.J. Arculus, S.M. Eggins, Laser ablation-inductively coupled plasma-mass spectrometry and tephra A new approach to understanding arc-magma genesis, *Geology* 27 (1999) 1119–1122.
- [15] N.J.G. Pearce, J.A. Westgate, W.T. Perkins, W.J. Eastwood, P. Shane, The application of laser ablation ICP-MS to the analysis of volcanic glass shards from tephra deposits bulk glass and single shard analysis, *Glob. Planet. Change* 21 (1999) 151–171.
- [16] J. Davidson, F. Tepley III, Z. Palacz, S. Meffan-Main, Magma recharge, contamination and residence times revealed by in situ laser ablation isotopic analysis of feldspar in volcanic rocks, *Earth Planet. Sci. Lett.* 184 (2001) 427–442.
- [17] J. Zachos, M. Pagani, L. Sloan, E. Thomas, K. Billups, Trends, rhythms, and aberrations in global climate 65 Ma to Present, *Science* 292 (2001) 686–693.
- [18] X. Barberá, L. Cabrera, M. Marzo, J.M. Parés, J. Agustí, A complete terrestrial Oligocene magnetobiostratigraphy from the Ebro Basin, Spain, *Earth Planet. Sci. Lett.* 187 (2001) 1–16.
- [19] A. Montanari, R. Drake, D.M. Bice, W. Alvarez, G.H. Curtis, B.D. Turrin, D.J. DePaolo, Radiometric time scale for the upper Eocene and Oligocene based on K/Ar and Rb/Sr dating of volcanic biotites from the pelagic sequences of Gubbio, Italy, *Geology* 13 (1985) 596–599.
- [20] K.G. Miller, J.D. Wright, R.G. Fairbanks, Unlocking the ice house: Oligocene-Miocene oxygen isotopes, eustasy, and margin erosion, *J. Geophys. Res.* 96 (1991) 6829–6848.
- [21] S. Pekar, K.G. Miller, New Jersey Oligocene 'Icehouse' sequences (ODP Leg 150X) correlated with global $\delta^{18}\text{O}$ and Exxon eustatic records, *Geology* 24 (1996) 567–570.
- [22] O.V. Pinous, M.A. Akhmetiev, D.L. Sahagian, Sequence stratigraphy and sea-level history of Oligocene strata of the northern Aral Sea region (Kazakhstan): Implications for glacioeustatic reconstructions, *Geol. Soc. Am. Bull.* 111 (1999) 1–10.
- [23] M. Huuse, O.R. Clausen, Morphology and origin of major Cenozoic sequence boundaries in the eastern North Sea Basin top Eocene, near-top Oligocene and the mid-Miocene unconformity, *Basin Res.* 13 (2001) 17–41.
- [24] M.A. Kominz, S.F. Pekar, Oligocene eustasy from two-dimensional sequence stratigraphic backstripping, *Geol. Soc. Am. Bull.* 113 (2001) 291–304.

- [25] Shipboard Scientific Party, Site 711, ODP Initial Reports 115 (1988) 657–732.
- [26] H. Okada, Quaternary and Paleogene calcareous nannofossils, ODP Sci. Results 115 (1990) 129–174.
- [27] S.G. Robinson, Applications for whole core magnetic susceptibility measurements of deep-sea sediments Leg 115 results, ODP Sci. Results 115 (1990) 737–771.
- [28] P. Mohr, Ethiopian flood basalts, *Nature* 303 (1983) 577–584.
- [29] P. Mohr, B. Zanettin, The Ethiopian flood basalt province, in: MacDougall (Ed.), *Continental Flood Basalts*, Kluwer, Dordrecht, 1988, pp. 63–110.
- [30] B. Zanettin, A. Gregnanin, E. Justin-Visentin, M. Nicoletti, C. Petrucciani, E.M. Piccirillo, L. Tolomeo, Migration of the Oligocene-Miocene ignimbritic volcanism in the Central Ethiopian Plateau, *N. Jb. Geol. Paläont. Mh.* 9 (1974) 567–574.
- [31] I. McDougall, W.H. Morton, M.A.J. Williams, Ages and rates of denudation of traps series basalts at Blue Nile Gorge, Ethiopia, *Nature* 254 (1975) 207–208.
- [32] P.W. Jones, Ages of the lower flood basalts of the Ethiopian plateau, *Nature* 261 (1976) 567–569.
- [33] V. Courtillot, R. Armijo, P. Tapponnier, Kinematics of the Sinai triple junction and two-phase model of Arabi-Africa rifting, in: M.P. Coward, J.F. Devey, O.L. Hancock (Eds.), *Continental Extensional Tectonics*, Geol. Soc. Lond. Spec. Publ. 28 (1987) 361–374.
- [34] R.S. White, D.P. McKenzie, Mantle plumes and flood basalts, *J. Geophys. Res.* 100 (1995) 17543–17585.
- [35] D. Ayalew, *Pétrologie et géochimie des ignimbrites des hauts plateaux éthiopiens: source, chronologie et impact environmental*, Ph.D. thesis, Institute National Polytechnique de Lorraine, Nancy, 1999, 191 pp.
- [36] D. Ayalew, P. Barbey, B. Marty, L. Reisberg, G. Yirgu, R. Pik, Source, genesis and timing of giant ignimbrite deposits associated with Ethiopian continental flood basalts, *Geochim. Cosmochim. Acta* 66 (2002) 1429–1448.
- [37] J.A. Baker, Stratigraphy, geochronology and geochemistry of Cenozoic volcanism in western Yemen, Ph.D. thesis, Royal Holloway University of London, 1996, 386 pp.
- [38] M. Menzies, K. Gallagher, A. Yelland, A. Hurford, Volcanic and non-volcanic rifted margins of the Red Sea and Gulf of Aden: Crustal cooling and margin evolution in Yemen, *Geochim. Cosmochim. Acta* 61 (1997) 2511–2527.
- [39] J.A. Baker, M.A. Menzies, M.F. Thirlwall, C.G. Macpherson, Petrogenesis of a Quaternary intraplate volcanic field, Yemen: Implications for plume-lithosphere interaction and polybaric melt hybridisation, *J. Petrol.* 38 (1997) 1359–1390.
- [40] I. Ukstins Peate, Volcanostratigraphy, geochronology and geochemistry of silicic volcanism in the Afro-Arabian flood volcanic province (Yemen and Ethiopia) Ph.D. thesis, Royal Holloway University of London, 2003, 412 pp.
- [41] B.J.A. Willigers, J.A. Baker, E.J. Krogstad, D.W. Peate, Precise and accurate in situ Pb-Pb dating of apatite, monazite, and sphene by laser ablation multiple-collector ICP-MS, *Geochim. Cosmochim. Acta* 66 (2002) 1051–1066.
- [42] J.A. Baker, S. Stos, T. Waight, Lead isotope analysis of archaeological metals by multiple-collector inductively coupled plasma mass spectrometry, *Archaeometry* (2002) submitted.
- [43] J.A. Baker, T.E. Waight, C. Meyzen, Pb isotope analysis of standards and samples using Tl and a ^{207}Pb - ^{204}Pb spike on a double focusing MC-ICPMS, *Chem. Geol.* (2002) submitted.
- [44] J.A. Baker, T. Waight, D. Ulfbeck, Rapid and highly reproducible analysis of rare earth elements by multiple collector inductively coupled plasma mass spectrometry, *Geochim. Cosmochim. Acta* 66 (2002) 3635–3646.
- [45] D. Ulfbeck, J.A. Baker, T.E. Waight, E. Krogstad, Rapid sample digestion by flux fusion and chemical separation of Hf for isotopic analysis by MC-ICP-MS, *Talanta* 59 (2003) 365–373.
- [46] S.R. Hart, A large-scale isotope anomaly in the southern hemisphere mantle, *Nature* 309 (1984) 753–757.
- [47] B.H. Baker, P.A. Mohr, L.A.J. Williams, Geology of the Eastern Rift System of Africa, *Geol. Soc. Am. Spec. Publ.* 186 (1972) 67 pp.
- [48] F. Walker, L.O. Nicolaysen, The petrology of Mauritius, *Colon. Geol. Miner. Resour.* 4 (1954) 3–43.
- [49] B.G.J. Upton, W.J. Wadsworth, The basalts of Réunion Island, Indian Ocean, *Bull. Volcanol.* 29 (1966) 7–23.
- [50] M.W. White, M.M. Cheatham, R.A. Duncan, Isotope geochemistry of Leg 115 basalts, *Proc. ODP Sci. Res.* 115 (1990) 23–42.
- [51] S.B. Keith, Paleosubduction geometries inferred from Cretaceous and Tertiary magmatic patterns in southwestern North America, *Geology* 6 (1978) 516–521.
- [52] F.W. McDowell, R.L. Mauger, K-Ar and U-Pb zircon chronology of Late Cretaceous and Tertiary magmatism in central Chihuahua State, Mexico, *Geol. Soc. Am. Bull.* 106 (1994) 118–132.
- [53] B. Martiny, R.G. Martinez-Serrano, D.J. Moran-Zenteno, C. Macias-Romo, R.A. Ayuso, Stratigraphy, geochemistry and tectonic significance of the Oligocene magmatic rocks of western Oaxaca, southern Mexico, *Tectonophysics* 318 (2000) 71–98.
- [54] J.A. Baker, M.F. Thirlwall, M.A. Menzies, Sr-Nd-Pb isotopic and trace element evidence for crustal contamination of plume-derived flood basalts: Oligocene flood volcanism in western Yemen, *Geochim. Cosmochim. Acta* 60 (1996) 2559–2581.
- [55] P. Riisager, J. Baker, I.A. Ukstins, Paleomagnetic and anisotropy of magnetic susceptibility studies of Oligocene flood volcanism in Yemen, *EOS J. Conf. Abstr.* 82(47) (2001) GP11A-0195.
- [56] Y. Touchard, P. Rochette, M.P. Aubry, F. Bassinot, Clues of a potential global climate impact of the Ethiopian Traps activity at 30 Ma, *EGS J. Conf. Abstr.* 26th General Assembly, 2001, CD.
- [57] S.P. Huestis, G.D. Acton, On the construction of geomagnetic timescales from non-prejudicial treatment of magnetic anomaly data from multiple ridges, *Geophys. J. Int.* 129 (1997) 176–182.

- [58] P.A. Baker, M.J. Malone, S.J. Burns, P.K. Swart, Minor element and stable isotopic composition of the carbonate fine fraction: Site 709, Indian Ocean, ODP Sci. Results 115 (1990) 661–675.
- [59] M.J. Le Bas, R.W. Le Maitre, A. Streckeisen, B. Zanettin, A chemical classification of volcanic rocks based on the total alkali-silica diagram, *J. Petrol.* 27 (1986) 745–750.
- [60] P.R. Renne, C.S. Swisher, A.L. Deino, D.B. Karner, T.L. Owens, D.J. DePaolo, Intercalibration of standards, absolute ages and uncertainties in $^{40}\text{Ar}/^{39}\text{Ar}$ dating, *Chem. Geol.* 145 (1998) 117–152.
- [61] E. Anders, N. Grevesse, Abundances of the elements: Meteoric and solar, *Geochim. Cosmochim. Acta* 53 (1989) 197–214.